JOURNAL OF COMPUTATIONAL PHYSICS **136,** 51–67 (1997)
ARTICLE NO. CP975729

Coupling Boltzmann and Navier–Stokes Equations by Half Fluxes

Patrick Le Tallec*,†,[1,3] and François Mallinger†,[2,3]

*Université Paris-Dauphine and *,†INRIA, Domaine de Voluceau, Rocquencourt, B.P. 105, Le Chesnay Cedex, France

Received October 16, 1996

We introduce an adaptative coupling of the Boltzmann and Navier–Stokes equations to compute hypersonic flows around a vehicle at high altitude. The coupling is achieved by matching half fluxes at the interface of the Boltzmann and Navier–Stokes domains. The domains are determined automatically by computing local kinetic residuals on a preliminary Navier–Stokes solution. Our method is developed here for monoatomic gases. Different numerical results illustrate its validity and limits.

1. INTRODUCTION

During the reentry phase, a spatial vehicle gets across different fluid regimes, characterized by the so-called Knudsen number. This dimensionless number is the ratio of the mean free path (the mean distance travelled by a particle between two successive collisions) by a characteristic length of the flow. At altitude of 90 km and up, the Knudsen number is large, corresponding to a rarefied regime. In this case the flow is computed by a kinetic model. At altitude below 70 km the Knudsen number is sufficiently small for the flow to be well described by the Navier–Stokes model. For intermediate altitude the Navier–Stokes equations cease to be valid; it is the transitional regime. At this level, slip effects can be observed in the boundary layer, and the gas gets rarefied in the wake. These modifications of the flow can be observed by kinetic calculations. Unfortunately, realistic kinetic simulations become rapidly too expensive, and often impossible, as the Knudsen number becomes smaller, because they require one computational cell per mean free path.

Different solutions have been proposed to compute such flows. The most standard uses analytical slip boundary conditions as described in [6, 28, 14]. Some difficulties arising from this method have led many authors to use intermediate asymptotic models such as the Burnett equation [29] and the Levermore model [17].

A different strategy has appeared in the last years. It consists in solving locally the kinetic model coupled with a global Navier–Stokes model. At first, the coupling was achieved by imposing friction boundary conditions on the obstacle [4]. This coupling requires that the Boltzmann and the Navier–Stokes domains include the obstacle as boundary, and the Navier–Stokes domain overlaps completely the Boltzmann domain. This strategy works well for very low Knudsen numbers but is always rather expensive. Moreover, rarefied effects are miscalculated by the Navier–Stokes solver when the Knudsen number increases.

In another direction, nonoverlapping coupling strategies have been proposed in [5, 18, 19], for handling more rarefied situations.

As an alternative, we propose here an adaptative half fluxes coupling. Our strategy answers two questions: how to couple the Boltzmann and the Navier–Stokes models, and where to do it. The coupling is achieved by matching half fluxes at the interface of the Navier–Stokes and Boltzmann domains. This condition results from a kinetic interpretation of the Navier–Stokes equations. To determine the Navier–Stokes domain, and consequently the Boltzmann domain, we introduce a criterion based on the analysis of kinetic validity of the numerical Navier–Stokes solution. Then we propose a global coupling algorithm, including an automatic definition of the domains and the time marching algorithm of [4]. Thanks to the half fluxes compatibility condition we can consider in the simulations Boltzmann and Navier–Stokes domains which do not overlap.

In the present paper, we briefly review the transition from the Boltzmann equation to the Navier–Stokes equations (Section 2) from which we derive formally the coupling strategy (Section 3). In Section 4, we describe the time marching algorithm, its implementation, and the Navier–Stokes and the Boltzmann solvers used in our simulations. In Section 5 we show first numerical results showing the limits of validity of the compatibility condition. In Section 6 we present the Grad criterion to determine the validity of the Navier–Stokes solution, which leads to the adaptative definition of the computational domains. We also proposed a global algorithm. Numerical results, which make use of the global algorithm, are presented in

[1] E-mail: Patrick.LeTallec@inria.fr.
[2] E-mail: mallinger@inria.fr.
[3] Supported by Hermes European Research Project and CEA-CESTA.

0021-9991/97 $25.00

Section 7. Finally we end this paper by concluding remarks.

2. BOLTZMANN EQUATION. KINETIC INTERPRETATION OF THE NAVIER–STOKES EQUATIONS

Let f be the density of the gas particles at position x, with velocity ξ, at time t. In adimensional form, the Boltzmann equation of rarefied gas dynamics characterizes this density as the solution of the integro-differential equation [6, 7, 9, 28],

$$\frac{\partial f}{\partial t} + \xi \cdot \frac{\partial f}{\partial x} = \frac{1}{\varepsilon} Q(f, f). \tag{1}$$

The collision operator Q counts the particles which are gained or lost through intermolecular collisions. For monoatomic gases, a phenomenological analysis leads to the following definition

$$Q(f, f) = \int_{\mathbb{R}^3 \times S^2} (f' f'_* - f f_*) B(|v_r|, |v_r \cdot \omega|)\, d\omega\, d\xi_*, \tag{2}$$

under the usual notation $f = f(\xi)$, $f_* = f(\xi_*)$, $f' = f(\xi')$, $f'_* = f(\xi'_*)$, with (ξ, ξ_*) and (ξ', ξ'_*) the pre- and postcollision particle velocities. The vector $v_r = \xi - \xi_*$ is the relative velocity of the pair of particles and $\omega \in S^2$ a vector of the unit sphere.

The collision cross section B measures the collision probability of particles with velocities ξ and ξ_*, and collision angle ω. If the collision is effective the postcollision velocities are deduced from the conservation of both momentum and kinetic energy, yielding

$$\begin{aligned} \xi' &= \xi + (v_r \cdot \omega)\omega, \\ \xi'_* &= \xi_* - (v_r \cdot \omega)\omega. \end{aligned}$$

The Knudsen number ε in (1) appears as a ratio between the characteristic times used to adimension the collision and advection terms, respectively.

The crucial point of our method is to use a kinetic interpretation of the Navier–Stokes equations. For this purpose we introduce an asymptotic model, approximating the Boltzmann equation, and degenerating to the Navier–Stokes model when the gas gets dense. This is achieved by the Chapman–Enskog theory, which writes f as a first-order expansion in ε,

$$\begin{aligned} f &= f_o(1 + \varepsilon\psi), \\ f_o &= \frac{\rho}{(2\pi RT)^{3/2}} \exp\left(-\frac{|\xi - u|^2}{2RT}\right), \end{aligned} \tag{3}$$

where f_o is the Maxwellian equilibrium distribution function and ψ is an unknown function. Introducing f in (1), it follows that ψ is the solution of

$$\psi = L^{-1}\left(\frac{\partial f_o}{\partial t} + \xi \cdot \frac{\partial f_o}{\partial x} + O(\varepsilon)\right), \tag{4}$$

where $L(\psi) = Q(f_o, f_o\psi) + Q(f_o\psi, f_o)$ is the linearized Boltzmann operator. The conservation laws are obtained replacing f by (3) in (1), multiplying by the collision vector $K = (1, \xi, |\xi|^2/2)$, and integrating over the velocity domain $\mathbb{R}^3$, yielding

$$\frac{\partial}{\partial t}\left(\int fK\, d\xi\right) + \frac{\partial}{\partial x} \cdot \left(\int \xi f K\, d\xi\right) = 0,$$

which writes

$$\frac{\partial}{\partial t}\begin{bmatrix} \rho \\ \rho u \\ \rho e_{tot} \end{bmatrix} + \frac{\partial}{\partial x}\begin{bmatrix} \rho u \\ \rho u \otimes u + pI - \tau \\ (\rho e_{tot} + p)u - \tau u + q \end{bmatrix} = 0, \tag{5}$$

under the notation

$$\begin{bmatrix} \rho \\ \rho u \\ \rho e_{tot} \end{bmatrix} = \int_{\mathbb{R}^3} \begin{pmatrix} 1 \\ \xi \\ |\xi|^2/2 \end{pmatrix} f\, d\xi,$$

$$\tau = -\int f_o \varepsilon \psi c \otimes c\, dc, \tag{6}$$

$$q = \int f_o \varepsilon \psi c |c|^2\, dc. \tag{7}$$

Here $c = \xi - u$, $e_{\text{tot}} = |u|^2/2 + e_{\text{int}}$ is the macroscopic total energy, and e_{int} the macroscopic internal energy.

The last step consists in calculating an approximation solution of ψ, in order to relate the viscous-stress tensor τ and the heat flux vector q to the lower macroscopic moments. At first order we obtain [6, 28],

$$\psi = \frac{a_o}{\sqrt{RT}}\left(\frac{|c|^2}{2RT} - \frac{5}{2}\right) c \cdot \frac{\partial T}{\partial x} + \frac{b_o}{RT}\left(c \otimes c - \frac{1}{3}|c|^2 I\right) : \frac{\partial u}{\partial x}, \tag{8}$$

where a_o and b_o are two constants. Replacing (8) in (6) and (7) we deduce the Navier–Stokes approximation of τ and q

$$\tau = \mu\left[\left(\frac{\partial u}{\partial x} + \frac{\partial u^t}{\partial x}\right) - \frac{2}{3}\operatorname{div} u I\right], \tag{9}$$

$$q = -\kappa \frac{\partial T}{\partial x}, \tag{10}$$

where $\mu = -\rho RT\varepsilon b_o$ and $\kappa = -\frac{5}{2}(a_o\varepsilon/\sqrt{RT})\rho(RT)^2$. The quantities a_o and b_o depend on the intermolecular potential of the collision (see [3, 28]).

Altogether, the Chapman–Enskog expansion produces the conservations form (5) of the Navier–Stokes equations, identifies the constitutive laws for τ and q, and gives in (8) an approximation of the underlying kinetic distribution, which is

$$f_{\mathrm{CE}} = f_o\left[1 + \frac{2}{5}\frac{q\cdot c}{\rho(RT)^2}\left(\frac{|c|^2}{2RT} - \frac{5}{2}\right) - \frac{1}{2}\frac{\tau : c\otimes c}{\rho(RT)^2}\right]. \tag{11}$$

Thus, rewriting the Navier–Stokes equations using the usual abstract conservative form

$$\frac{\partial U}{\partial t} + \frac{\partial F(U)}{\partial x} = 0,$$

we observe that the associated fluxes have the kinetic form

$$F(U) = \int \xi K\, f_{\mathrm{CE}}\, d\xi. \tag{12}$$

This kinetic form can also be obtained through different asymptotic expansions, such as in Grad [13] or Levermore [17].

3. BOLTZMANN NAVIER–STOKES COUPLING: FORMAL DERIVATION

We introduce first a formal Boltzmann–Boltzmann coupling by extending classical domain decomposition strategies [11, 8, 16] to the Boltzmann equation. Consider the Boltzmann equation (1) in the global domain $\Omega \times \mathbb{R}^3 \times [0, T]$, where the spatial domain Ω is an open bounded set in $\mathbb{R}^3$, the velocity domain is $\mathbb{R}^3$, and the time interval is $[0, T]$ with $T > 0$. We impose classical conditions on the boundary of $\Omega \times \mathbb{R}^3 \times [0, T]$. To get the coupled problem we first split the spatial domain into two nonoverlapping subdomains Ω_1 and Ω_2, as in Fig. 1, such that

$$\overline{\Omega} = \overline{\Omega}_1 \bigcup \overline{\Omega}_2, \quad \Omega_1 \bigcap \Omega_2 = \varnothing, \quad \overline{\Omega}_1 \bigcap \overline{\Omega}_2 = \Gamma.$$

The surface Γ is the interface between the domains Ω_1 and Ω_2. If f_i is the restriction of f in $\Omega_i \times \mathbb{R}^3 \times [0, T]$, the global problem is formally equivalent to the coupled problem

$$\begin{aligned} &\frac{\partial f_1}{\partial t} + \xi\cdot\frac{\partial f_1}{\partial x} = \frac{1}{\varepsilon}Q(f_1, f_1) \quad \text{in } \Omega_1 \times \mathbb{R}^3 \times (0, T), \\ &f_1 = f_2 \qquad\qquad\qquad\qquad \text{on } \Gamma^- \times [0, T], \end{aligned} \tag{13}$$

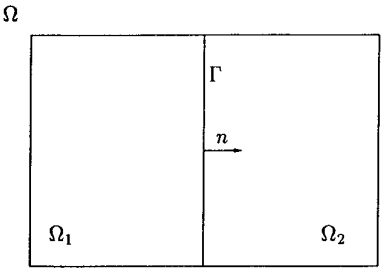

FIG. 1. Boltzmann splitted domain.

$$\begin{aligned} &\frac{\partial f_2}{\partial t} + \xi\cdot\frac{\partial f_2}{\partial x} = \frac{1}{\varepsilon}Q(f_2, f_2) \quad \text{in } \Omega_2 \times \mathbb{R}^3 \times (0, T), \\ &f_2 = f_1 \qquad\qquad\qquad\qquad \text{on } \Gamma^+ \times [0, T], \end{aligned} \tag{14}$$

where

$$\Gamma^+ = \{(x, \xi) \in \Gamma \times \mathbb{R}^3 / \xi\cdot n(x) > 0\},$$
$$\Gamma^- = \{(x, \xi) \in \Gamma \times \mathbb{R}^3 / \xi\cdot n(x) < 0\}.$$

The vector $n(x)$ denotes the normal vector to Γ at the point x, oriented from Ω_1 to Ω_2, as shown in Fig. 1. The matching conditions of (13) and (14) express that the distribution of particles coming in the subdomain Ω_1 (resp. Ω_2) is equal to the distribution of particles going out of the subdomain Ω_2 (resp. Ω_1).

The coupled problem (13), (14) can be solved by the following iterative procedure, which is proved to converge for pure hyperbolic problems [11],

- Guess $f_2(x, \xi, t)$ on incoming characteristics (i.e., $n(x)\cdot\xi < 0$);
- Solve the resulting subproblem in Ω_1;
- With the resulting value $f_1(x, \xi, t)$, imposed on incoming characteristics (i.e., $n(x)\cdot\xi > 0$), solve the subproblem on Ω_2;
- Use the result to update $f_2(x, \xi, t)$ on the interface and re-iterate.

At the present time we can prove the equivalence between the global and the coupled problems, when replacing the Boltzmann model by the BGK model. We think that the demonstration of convergence of the algorithm, in this BGK case, is not an insurmountable problem. We will present our results in a following paper.

In any case, it is easy to extend the above strategy to the Boltzmann–Navier–Stokes coupled problem. For this purpose we replace in the subdomain Ω_1, the distribution f_1 by its Navier–Stokes approximation f_{NS}, for example

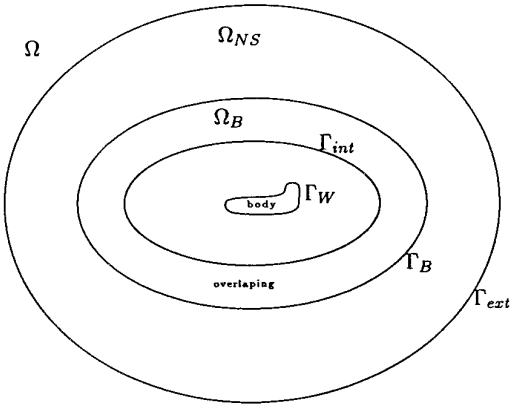

FIG. 2. Boltzmann Navier–Stokes split domain.

the Chapman–Enskog one. Thus the interface boundary conditions of (13) and (14) are transformed into

$$f_2(x, \xi, t) = f_{\mathrm{NS}}(x, \xi, t) \quad \text{on } \Gamma^+ \times [0, T], \tag{15}$$

$$f_{\mathrm{NS}}(x, \xi, t) = f_2(x, \xi, t) \quad \text{on } \Gamma^- \times [0, T]. \tag{16}$$

Condition (15) is imposed as the boundary condition in the Boltzmann model (14), on Ω_2. On Ω_1, we reduce our kinetic equations (13) and (16) to the Navier–Stokes equation by multiplication by the collision vector K and integration in velocity. We therefore have to solve the differential equation (5) on Ω_1, with constitutive laws (9), (10) and boundary conditions

$$F(U) \cdot n_{/\Gamma} = F(U)^+ \cdot n + F(U)^- \cdot n, \tag{17}$$

where the outgoing and ingoing fluxes are respectively given by

$$F(U)^+ \cdot n = \int_{\xi \cdot n > 0} K\xi \cdot n f_{\mathrm{NS}}(x, \xi, t)\, d\xi, \tag{18}$$

$$F(U)^- \cdot n = \int_{\xi \cdot n < 0} K\xi \cdot n f_2(x, \xi, t)\, d\xi. \tag{19}$$

After some calculation $F(U)^+ \cdot n$ can be expressed only in terms of the moments ρ, u, T, and their gradients. For the coupled problem, the compatibility conditions are finally given by (15) for the Boltzmann model and by (17)–(19) for the Navier–Stokes model. We usually call these conditions ''half flux conditions'' and the resulting coupling ''the half flux coupling.''

4. BOLTZMANN NAVIER–STOKES COUPLING: IMPLEMENTATION

4.1. *The Coupled Problem*

Let us consider in this section a more general geometry of an external flow around a flying vehicle (Fig. 2), closer to the geometry used in the computational test cases.

The Boltzmann domain Ω_{B} contains the body. The Navier–Stokes domain Ω_{NS} may overlap the Boltzmann domain ($\Gamma_{\mathrm{int}} \in \Omega_{\mathrm{B}}$), or not ($\Gamma_{\mathrm{int}} = \Gamma_{\mathrm{B}}$).

The coupled problem now consists in solving the following equations:

On Ω_{B} we solve the Boltzmann equation

$$\frac{\partial f}{\partial t} + \xi \cdot \frac{\partial f}{\partial x} = \frac{1}{\varepsilon} Q(f, f), \tag{20}$$

with boundary conditions

$$f(\xi)_{/\Gamma_B} = \rho M_{u,T}(\xi) \qquad \text{if } \xi \cdot n < 0,$$

$$f(\xi)_{/\Gamma_W} = k M_{u_W, T_W}(\xi) \quad \text{if } \xi \cdot n < 0 \text{ (perfect accommodation)},$$

where n denotes the outward normal vector to the boundary of Ω_{B}.

On Ω_{NS} we solve the Navier–Stokes equations

$$\frac{\partial U}{\partial t} + \frac{\partial}{\partial x} \cdot F(U) = 0,$$

with boundary conditions

$$U = U_\infty \qquad \text{at infinity},$$

$$F(U)^- \cdot n = \int_{\xi \cdot n} K\xi \cdot n f(x, \xi, t)\, d\xi \quad \text{on } \Gamma_{\mathrm{int}}.$$

There is a clear coupling between the above Boltzmann and the Navier–Stokes models. The coupling from Boltzmann to Navier–Stokes is achieved by imposing the incoming half fluxes $F^-(U) \cdot n$, predicted and computed by the Boltzmann solver. The outgoing fluxes $F^+(U) \cdot n$ are computed by the Navier–Stokes solver. Conversely the Navier–Stokes model acts on the Boltzmann model by imposing the incoming velocity distribution $\rho M_{u,T}$ on the interface Γ_{B}. The parameters ρ, u, and T of this distribution are predicted locally by the Navier–Stokes model. The reader can object that this Maxwellian distribution is only valid in regions of translational equilibrium, where the effects of viscosity and thermal conductivity are insignificant. To be more accurate, Lukschin [18] has proposed to predict f_2 on Γ^+ by the modified Chapman–Enskog expansion $\rho M_{u,T}(1 - \varepsilon/2\psi)^2$. In this way the velocity distribution is always a nonegative function; the velocity of particles being obtained by an acceptance rejection method.

Observe, also, that apart of any possible problem on the validity of the Navier–Stokes model, there is no restriction on the location of the interface Γ_{int}. This is precisely a considerable advantage of the half fluxes coupling, compared with coupling by friction. Moreover, the Navier–

Stokes solver is not concerned anymore about the boundary conditions on the body since they are treated by the Boltzmann solver.

4.2. *Compatibility between the Boltzmann and Navier–Stokes Models*

The compatibility is achieved through a proper choice of the viscosity model. At the microscopic level the choice of the intermolecular potential determines the macroscopic law of viscosity. This dependence appears in the study of the transition from Boltzmann to Navier–Stokes. In the simulations we will consider, for the Boltzmann collision operator, the "variable hard sphere" model

$$B = C|v_r|^{1-\alpha},$$

where C is a constant which leads to the Sutherland viscosity law for the Navier–Stokes equations,

$$N = KT^{1/2+\alpha},$$

where K is a constant.

4.3. *The Coupling Algorithm*

To solve the coupled problem we will use the time marching algorithm introduced in [5, 4]. The time loop reduces to the following sequence of operations:

1. Solve a few steps of the local Boltzmann solver

$$\frac{f^n - f^{n-1}}{\Delta t} + \operatorname{div}_x(\xi f^n) = Q(f^n, f^n)(x, \xi) \quad \text{in } \Omega_B,$$

$$f^n(x, \xi) = f_{\mathrm{NS}}^{t_{n-1}}(x, \xi) \quad \text{on } \Gamma_B \quad \text{if } \xi \cdot n > 0,$$

$$f^n = \text{Maxwellian on the body;}$$

2. From f^n, compute the half fluxes $F^-(U^n)$, entering the internal boundary of the Navier–Stokes region;

3. With these imposed fluxes $F^-(U^n)$, using the boundary condition (17) on the interface and usual boundary conditions at infinity, integrate the Navier–Stokes equations a few steps in time on the external domain and go back to the Boltzmann problem.

Remark 4.1. In the computational tests we stop the algorithm as soon as the boundary conditions on Γ_{B} are stationary, i.e., when the parameters of the Maxwellian distribution are stationary. For example, we can control the density through the residual

$$\frac{\sum_{x_i \in \Gamma_{\mathrm{B}}} |\rho_i^{n+1} - \rho_i^n|}{\sum_{x_i \in \Gamma_{\mathrm{B}}} \rho_i^0}, \tag{21}$$

where ρ^0 is the initial density.

4.4. *Navier–Stokes Solver*

The Navier–Stokes code used in our simulations is based on a least squares Petrov–Galerkin finite element method. This code was developed at Dassault Aviation Company. Introducing the entropic change of variables [21],

$$V = \frac{\partial}{\partial U} H = \frac{1}{\rho e_{int}} \begin{pmatrix} -\rho e_{tot} + \rho e_{int}(\gamma + 1 - s) \\ \rho u_1 \\ \rho u_2 \\ -\rho \end{pmatrix},$$

where $H = H(U) = -\rho \ln (p\rho^{-\gamma})$ is the entropy function, the Navier–Stokes equations become

$$\tilde{A}_0 V_{,t} + \tilde{A}_i V_{,i} - (\tilde{K}_{ij} V_{,j})_{,i} = L(V) = 0. \tag{22}$$

The matrices $\tilde{A}_0$, $\tilde{A}_i$, $\tilde{K}_{ij}$ are symmetric and $\tilde{A}_0$, $\tilde{K}_{ij}$ are respectively strictly positive and semipositive. The discrete solution of any Galerkin approximation of the system (22) automatically satisfies the second law of thermodynamics.

The discretization is achieved by a time discontinuous Galerkin method, resulting in a complete space time finite element method, applied to the symmetric Navier–Stokes equations (22); see [25, 21]. A least square operator and a discontinuity capturing operator are added to ensure the stability of the method, especially next to shock waves or boundary layers. For this purpose, following Shakib [25], we introduce a partition of the time interval $[0, T] = \bigcup_{n=0}^{N} I_n$, where $I_n = [t_n, t_{n+1}]$, and a partition of the spatial domain Ω in N_e elements Ω_{n_e}. Then a space time element is defined by $Q_{n_e}^n = \Omega_{n_e} \times I_n$. With the notations $Q_n = \Omega \times I_n$ and $P_n = \Gamma \times I_n$, the spaces of trial functions $\mathscr{S}_n^h$ and weighting functions $\mathscr{W}_n^h$ are

$$\mathscr{S}_n^h = \{V^h / V^h \in (C^0(Q_n))^m, V^h_{/Q_n^e} \in (P_k(Q_n^e))^m, q(V^h) = g(t) \text{ sur } P_n\},$$

$$\mathscr{W}_n^h = \{W^h / W^h \in (C^0(Q_n))^m, W^h_{/Q_n^e} \in (P_k(Q_n^e))^m, q'(W^h) = 0 \text{ sur } P_n\},$$

where m is the number of local degrees of freedom, q is the nonlinear boundary condition transformation function, g is the prescribed boundary condition [25], and P_k is the set of kth-order polynomials.

The finite element variational formulation of (22) is then written as follows:

• Within each Q_n, $n = 0, ..., N - 1$, find $V^h \in \mathscr{S}_n^h$ such that for all $W^h \in \mathscr{W}_n^h$, the following equation is satisfied:

$$\int_{Q_n} (-W_{,t}^h \cdot U(V^h) - W_{,i}^h \cdot F_i^c(V^h) + W_{,i}^h \cdot \tilde{K}_{ij} V_{,j}^h)\, dQ$$
$$+ \int_\Omega (W^h(t_{n+1}^-) \cdot U(V^h(t_{n+1}^-)) - W^h(t_n^+) \cdot U(V^h(t_n^-)))\, d\Omega$$
$$+ \sum_{e=1}^{(n_e)_n} \int_{Q_n^e} (L(W^h) \cdot \tau L(V^h))\, dQ \qquad (23)$$
$$+ \sum_{e=1}^{(n_e)_n} \int_{Q_n^e} DC(W^h, V^h)\, dQ$$
$$= \int_{P_n} W^h \cdot (-F_i^c(V^h) + F_i^d(V^h)) \cdot n_i\, dP.$$

We refer to [21, 25] for the details concerning the matrix τ and the operator DC.

The finite elements generally used are piecewise linear in space and constant or linear in time. Both discretizations lead to a system of nonlinear algebraic equations at every time step. A linearization is performed which leads to nonsymmetric linear systems solved by a linear GMRES iterative method with a symmetric block diagonal preconditioning described in [25, 26].

The coupling compatibility condition on Γ_{int} consists in replacing $F(U)$, in the Galerkin boundary term of (23), by $F^+(U) + F^-(U)$, with $F^-(U^n)$ imposed by the Boltzmann solver.

Remark 4.2. It is obvious that the new boundary condition (17) could be implemented in a similar way in a finite volumes solver. Numerical results can be found in [5] for the Boltzmann–Euler coupling, using a finite volumes code to solve the Euler equations. In this particular case, the Chapman–Enskog distribution is replaced by the Maxwellian distribution or by some well chosen functions with compact support.

4.5. *Boltzmann Solver*

The algorithm we use is based on the "finite poinset method" due to Neuzert *et al.* [23, 15]. It is an extension of Nanbu's algorithm [22]; see also [1, 2] for theoretical investigations. The main idea consists in decoupling the physical process in a free transport phase and a collision phase. Thus we successively solve the free transport equation,

$$\frac{\partial f}{\partial t} + \xi \cdot \frac{\partial f}{\partial x} = 0, \qquad (24)$$

and the homogeneous collision equation,

$$\frac{\partial f}{\partial t} = Q(f, f). \qquad (25)$$

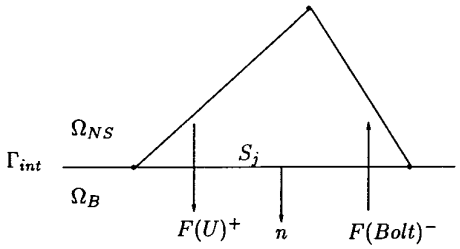

FIG. 3. Navier–Stokes coupling boundary condition. The half flux $F(\text{Bolt})^-$ is computed by the Boltzmann solver.

The particle approximation is based on the approximation of the density f by a sum of Dirac masses

$$f(t, x, \xi) \simeq \frac{1}{n_\infty} \sum_{i=1}^{N} \delta(x - x_i(t)) \delta(\xi - \xi_i(t)), \qquad (26)$$

where N denotes the total number of numerical particles.

For each time step, the transport equation is solved by advancing the particles in space using the velocity of the preceding time step. Then the global domain is subdivided in regular cells C_j and the collision step is solved separately on each cell. The collision probability is calculated with the VHS model. The collisions with the body are performed with specular reflexion or reflexion with accomodation. For details see the above references, [24], or [5].

For the coupling strategy we need to compute in this algorithm the fluxes $F(\text{Bolt})^- \cdot n$ crossing the interface Γ_{int}, from the Boltzmann to the Navier–Stokes domain. For this purpose the interface is subdivided in segments S_j (see Fig. 3). The flux $F(\text{Bolt})^-$, during the time unit, is then

$$F(\text{Bolt})^- \cdot n = \frac{1}{\Delta t\, \Delta l} \int_{[t,\Delta t]} dt \int_{\text{Seg}} dx \int_{\xi \cdot n \le 0} f_B \begin{pmatrix} 1 \\ \xi \\ \frac{|\xi|^2}{2} \end{pmatrix} \xi \cdot n\, d\xi \qquad (27)$$
$$= \frac{1}{\Delta t\, \Delta l} \left[\sum_{\{i, \xi_i \cdot n < 0\}} \right] \begin{pmatrix} 1 \\ \xi_i \\ \frac{|\xi_i|^2}{2} \end{pmatrix},$$

where l_j is the length of the segment S_j.

Remark 4.3. In order to minimize the memory requirements, at each call to the Boltzmann solver, we initialize, in each cell C_j, the distribution of particles by the Maxwellians M_j whose parameters ρ_j, u_j, and T_j are computed in the previous call to the Boltzmann solver.

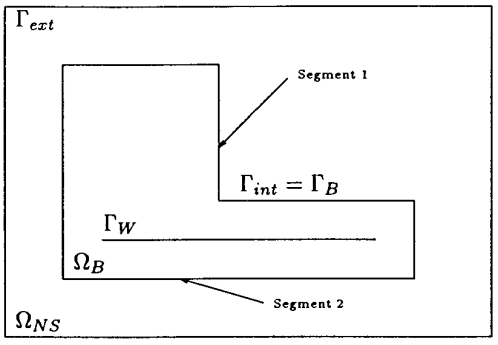

FIG. 4. Geometry for the validity test cases.

5. NUMERICAL RESULTS: LIMIT OF VALIDITY

In this section our goal is to show the limits of validity of the half fluxes condition and the importance of a proper localisation of the boundary Γ_{int}. The geometry of the present test cases is as in Fig. 4. We introduce in this geometry serious difficulties: segment 1 is perpendicular to the shock and segment 2 is almost tangent to it.

The following parameters are kept constant in all test cases,

$M_\infty = 18.33$,
$T_\infty = 13.6\ K$, angle of attack = 0,
$u_\infty = 1503\ m/s$, plate length = $1\ m$,
$T_W = 290\ K$,

while the Knudsen number, measuring the rate of rarefaction of the gas at infinity, and the parameter ω, connecting the VHS model of collision to the macroscopic viscosity, vary:

test 1: $\omega = 0.75$, $\varepsilon = 1.16E-02$,
test 2: $\omega = 0.75$, $\varepsilon = 5.32E-03$,
test 3: $\omega = 0.75$, $\varepsilon = 5.32E-04$,
test 4: $\omega = 0.5$, $\varepsilon = 5.32E-02$,
test 5: $\omega = 0.5$, $\varepsilon = 1.16E-02$,
test 6: $\omega = 0.5$, $\varepsilon = 5.32E-03$.

Figures 5 to 10 represent the Mach isolines for each of these tests.

We can remark first, looking only at the Boltzmann solutions, that the shock thickness increases as the parameter ω or the Knudsen number increase. Moreover, the quality of the coupled solution deteriorates when the shock thickness increases. Tests 1, 2, and 4 show that the coupled solutions are not satisfactory. For all these tests we notice that the angle between the shock, which crosses segment 1, and the plate is always preserved, but that the shock thickness is not preserved at the interface. Owing to the direction of the flow, this poor interface matching has small effect on the Boltzmann solution. The situation is more dramatic at the interface defined by segment 2. Indeed the isolines are there completely discontinuous.

Otherwise the coupled solutions are pretty good for the

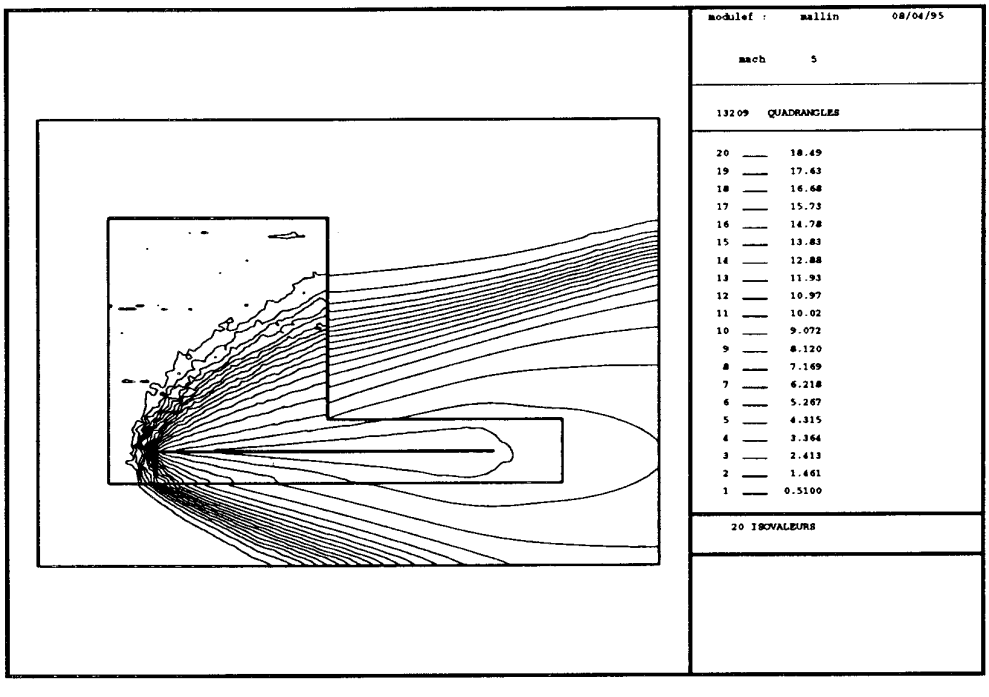

FIG. 5. Iso-Mach lines, $\omega = 0.75$, $Kn = 1.16E-02$.

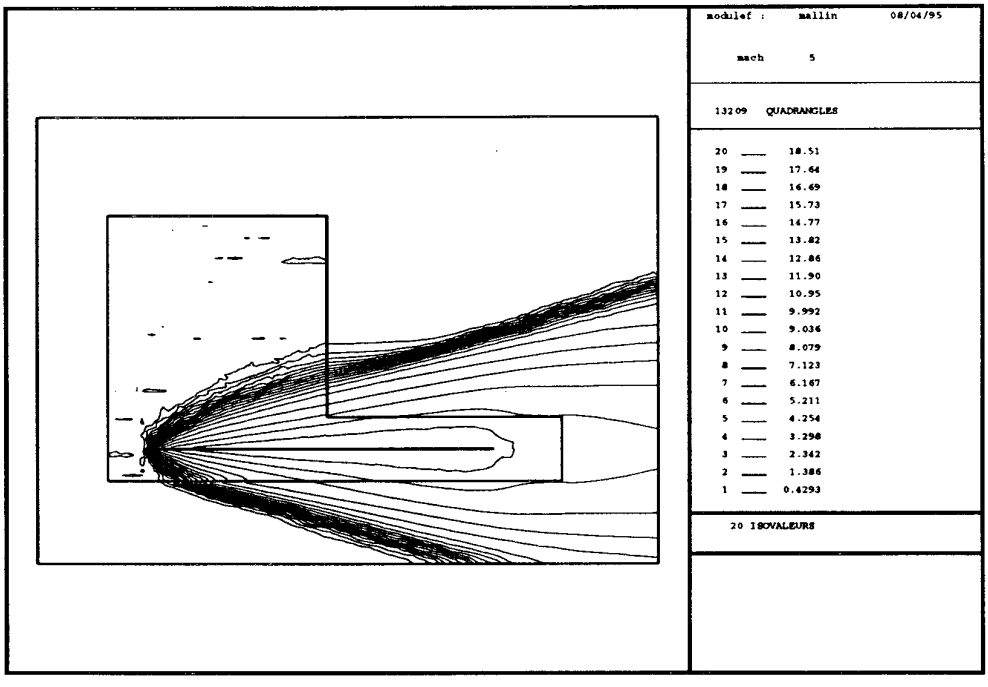

FIG. 6. Iso-Mach lines, $\omega = 0.75$, $Kn = 5.32E - 03$.

tests 3, 5, and 6: no variation of shock thickness at the interface and good isolines continuity. Therefore, it appears clearly that the coupled solution is better when the shock is thin. Moreover, the interface condition seems to be more sensitive to the size of the nonequilibrium surface than to the nonequilibrium itself. As a consequence it is not possible to choose the interface, or equivalently, the Boltzmann and Navier–Stokes domains, without care. In

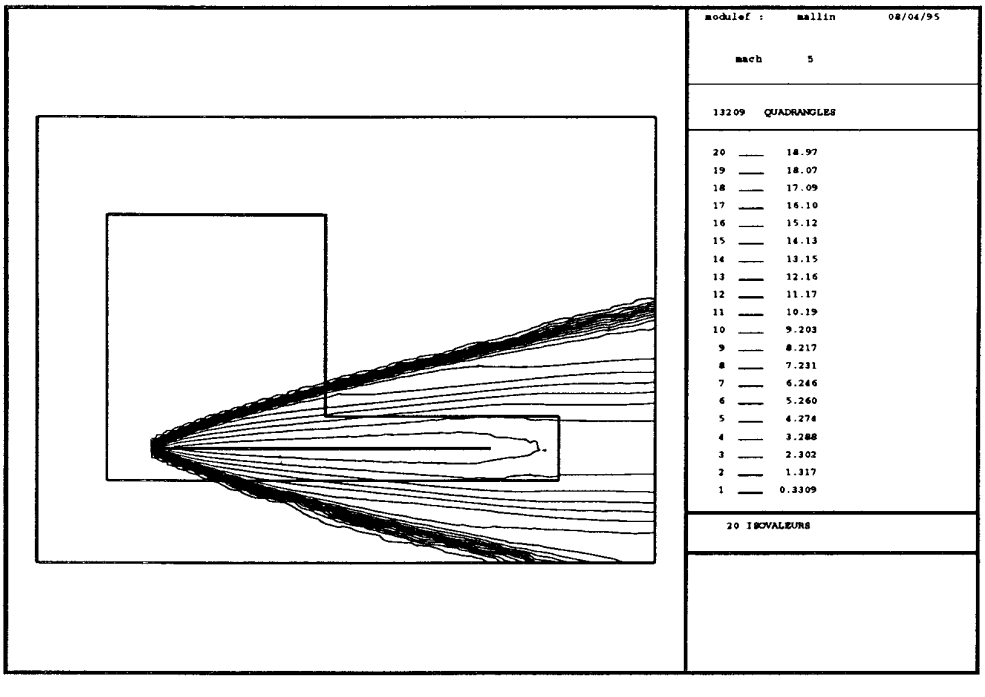

FIG. 7. Iso-Mach lines, $\omega = 0.75$, $Kn = 5.32E - 04$.

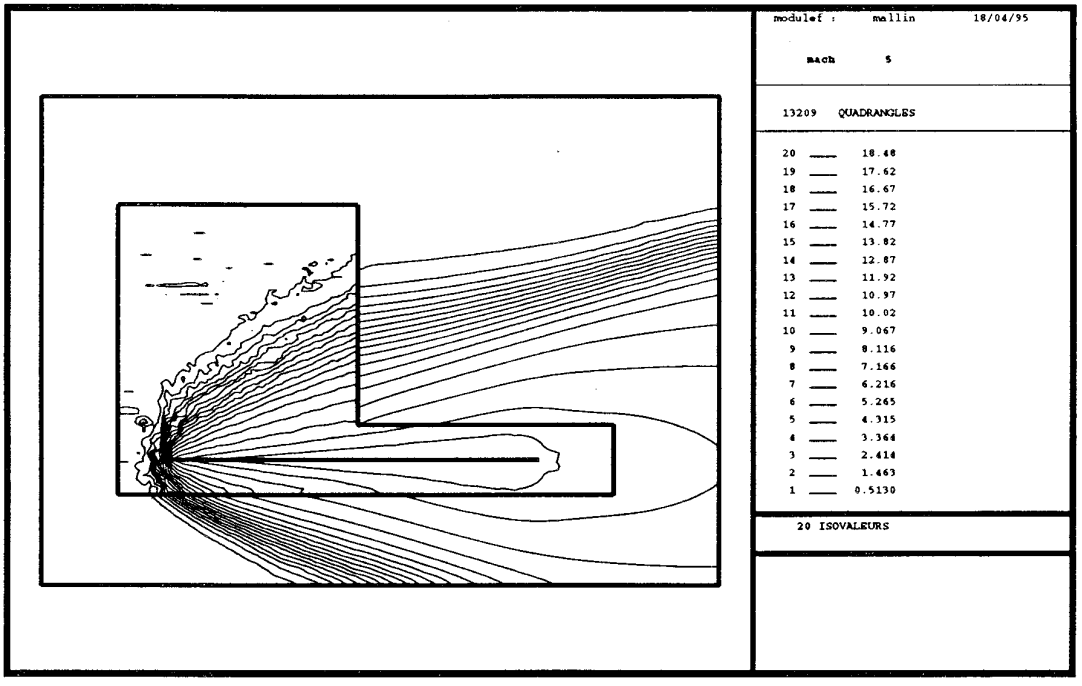

FIG. 8. Iso-Mach lines, $\omega = 0.5$, $Kn = 5.32E - 02$.

addition, we can see here that the Knudsen number at infinity is not a good parameter for this choice. It is necessary to perform a preliminary study to determine where the flow may be modelled by the Navier–Stokes equations. This problem is investigated in the following section.

6. GRAD CRITERION. GLOBAL ADAPTATIVE ALGORITHM

6.1. *Derivation of the Grad Criterion*

We propose in this section a method to determine the validity of a numerical Navier–Stokes solution and to obtain a correct definition of the Navier–Stokes domain or equivalently of the interface boundary Γ_{int} $(= \Gamma_{\text{B}})$. Our strategy is based on the analysis of the residual of the Grad thirteen moment equations.

More precisely, for a given known Navier–Stokes solution, we compute the moments $K_G = (1, \xi, \xi \otimes \xi, |\xi|^2\xi)$ of the Boltzmann equation for the corresponding Grad Chapman–Enskog distribution (11),

$$R_{\text{NS}} = \int K_{\text{G}} \left(\frac{\partial f_{CE}}{\partial t} + \xi \cdot \frac{\partial f_{CE}}{\partial x} - Q(f_{\text{CE}}) \right) d\xi = \frac{\partial V_{\text{NS}}}{\partial t} + \frac{\partial F(V_{\text{NS}})}{\partial x} - J(V_{\text{NS}}), \tag{28}$$

under the notation (given here for the hard sphere collision model)

$$V_{\text{NS}} = \begin{pmatrix} \rho \\ \rho u_i \\ \rho u_i u_j - \sigma_{ij} \\ 2\rho E u_i - 2u_k \sigma_{ik} + S_i \end{pmatrix},$$

$$F(V_{\text{NS}}) = \begin{pmatrix} \rho u_k \\ \rho u_i u_k - \sigma_{ik} \\ \rho u_i u_j u_k - (\sigma_{ki} u_j + \sigma_{jk} u_i + \sigma_{ij} u_k) + \frac{1}{5}(\delta_{ki} S_j + \delta_{jk} S_i + \delta_{ij} S_k) \\ (S_i - 2\sigma_{il} u_l + 2\rho E u_i) u_k - 2\,RT\,p\,\delta_{ik} - 2u_l u_i \sigma_{kl} - (7\,RT + u^2)\sigma_{ik} + \frac{7}{5} u_i S_k + \frac{2}{5}(S_i + S_l u_l \delta_{ki}) \end{pmatrix},$$

$$J(V_{\text{NS}}) = \begin{pmatrix} 0 \\ 0 \\ \sqrt{\frac{\pi}{RT}} \left(\frac{16\sigma^2}{5m} \tau_{ij} + \frac{8\sigma^2}{105mp} (\delta_{ij} \tau_{rs} \tau_{rs} - 3\tau_{ir} \tau_{jr}) - \frac{\sigma^2}{375mpRT} (3S_i S_j - S_r S_r) \right) \\ -\frac{32\sigma^2}{15m} \frac{\sqrt{\pi}}{RT} S_i + \frac{8}{25} \frac{\sqrt{\pi}}{pRT} \tau_{ir} S_r \end{pmatrix},$$

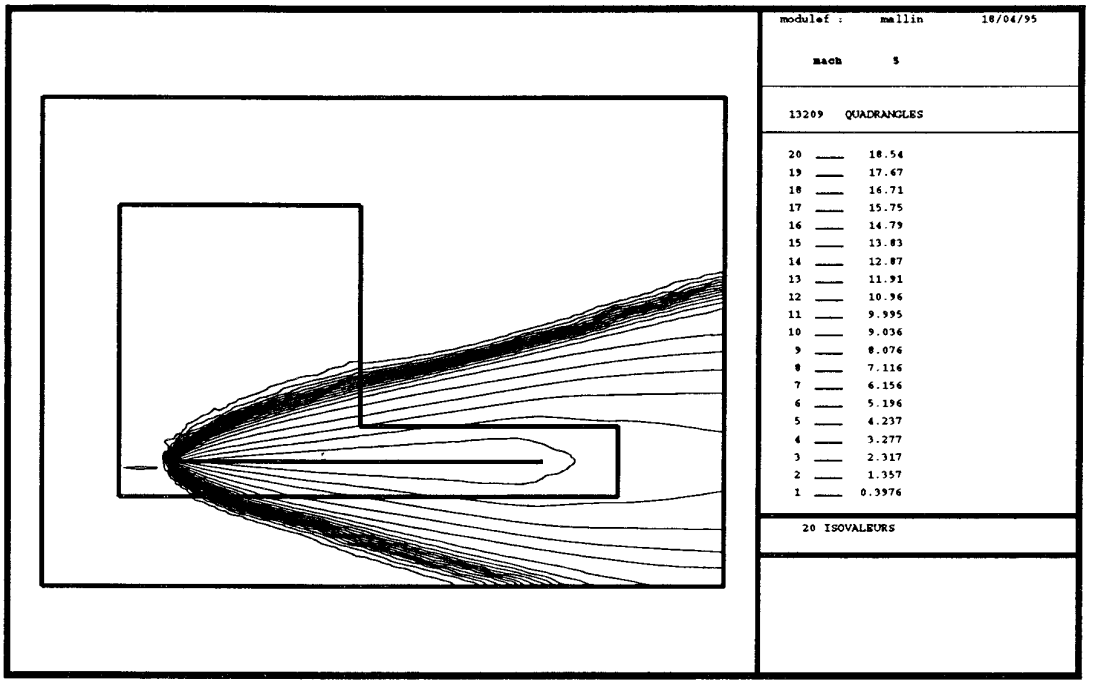

FIG. 9. Iso-Mach lines, $\omega = 0.5$, $Kn = 1.16E - 02$.

where σ^2 is the diameter of molecule protection sphere, m the mass of a molecule, and $S_i = 2q_i$.

If the Navier–Stokes distribution is a good approximation of the Boltzmann solution, the above residual R_{NS} will be close to zero. Therefore, the Navier–Stokes solution will be valid everywhere the residual is small.

In practice we compute R_ψ, where ψ is a component of the vector K_{G}, in a weak form by a finite element proce-

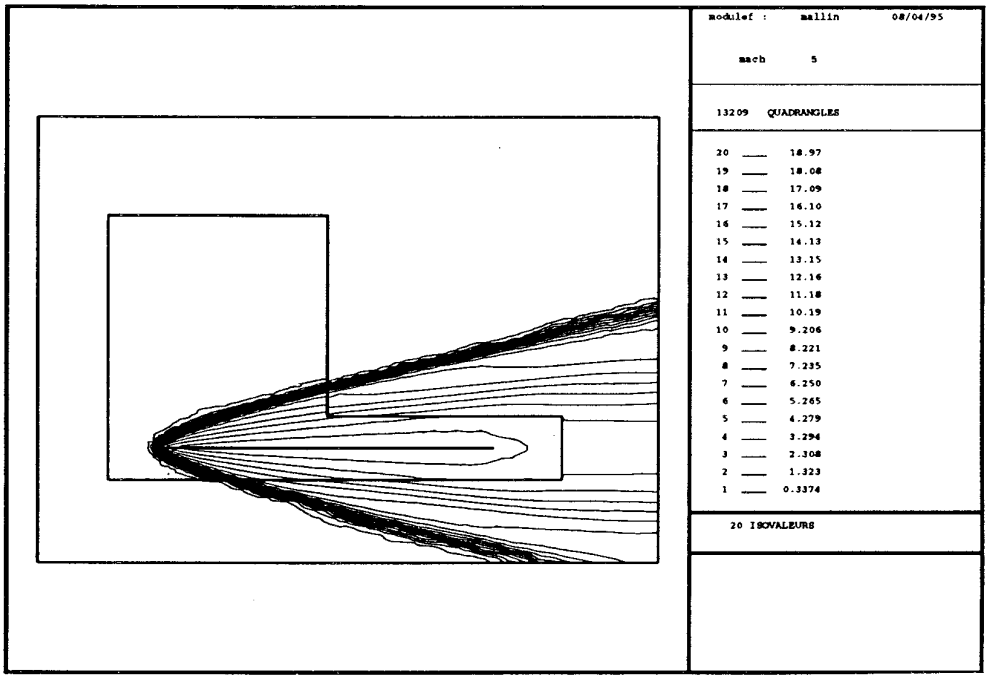

FIG. 10. Iso-Mach lines, $\omega = 0.5$, $Kn = 5.32E - 03$.

dure. More precisely, in the numerical tests of the following section we compute $\|R_{v_i v_j}\|_{l^2}$. We call this method the Grad criterion.

6.2. *The Resulting Adaptative Algorithm*

Our global adaptative algorithm now consists of two steps; an initializing step, developed in this section, and a coupling step, identical to the coupling algorithm introduced in Section 3.

The initialization algorithm is the following:

1. Compute a Navier–Stokes solution, with slip or no slip boundary conditions on the body, on the global domain;

2. Compute the Grad residual R_{NS} on the global domain;

3. Determine the region where the Navier–Stokes solution is valid.

For this purpose, we fix a threshold value of the Grad residual. Then, on each node of the global Navier–Stokes mesh, if the Grad residual value is smaller than the threshold value the Navier–Stokes solution is valid; if not this point is introduced in the Boltzmann domain. The main difficulty is precisely the evaluation of this threshold value. There is no automatic method to determine this number; its choice is always empiric;

4. Determine the internal boundary Γ_{int} of the reduced Navier–Stokes domain;

5. Remesh the new Navier–Stokes domain, using the Navier–Stokes solution of step 1.

To remesh the new Navier–Stokes domain, we use an anisotropic mesh generator. The resulting mesh is of Voronoi type and equidistributes the mesh nodes according to a metric associated to the second derivatives of the step 1 Navier–Stokes solution.

Figure 11 gives an example of the resulting geometry.

Remark 6.1. It is possible to introduce an adaptative updating of the domains in the time marching algorithm. The Navier–Stokes domain could be reevaluated after each global Navier–Stokes iteration.

7. NUMERICAL RESULTS: ADAPTATIVE COUPLING

7.1. *Flow around an Ellipse*

We consider in this section a hypersonic flow around an ellipse with a 30° angle of attack. More precisely we choose the following parameters:

$$M_\infty = 20, \qquad T_W = 1000\ \mathrm{K},$$
$$T_\infty = 167.3\ \mathrm{K}, \quad \mathrm{Re}_{/\mathrm{m}} = 5000,$$

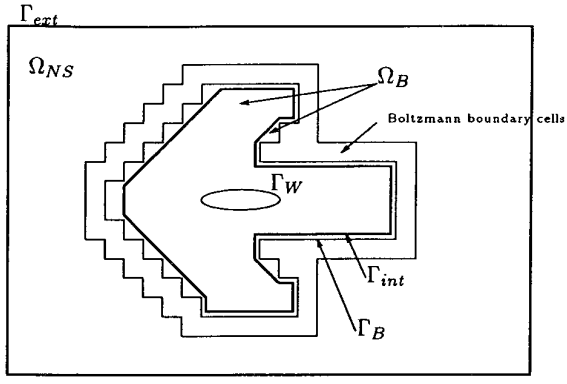

FIG. 11. Global domain splitting: Boltzmann and Navier–Stokes domains. In the implementation, the Boltzmann domain is the set of all rectangular cells on which the Grad residual is large. The Navier–Stokes domain is obtained by a smooth "conservative" interpolation of the boundary of the Boltzmann domain, adding a small overlap in order to avoid any "hole" in the partition.

$$u_\infty = 5672\ \mathrm{m/s}, \qquad \gamma = 5/3,$$
$$\rho_\infty = 1 \qquad\qquad \mathrm{Pr} = 2/3.$$

The computational domains are obtained by the algorithm of Section 6.2. The Navier–Stokes mesh is made up 1758 nodes and 3233 triangles (Fig. 12). The Navier–Stokes algorithm is advanced for each global iteration of 500 explicit time steps with a CFL number equal to 0.1.

The first global Boltzmann iteration is initialized by a Maxwellian with parameters given by the initial Navier–Stokes solution. For a global Boltzmann iteration, the Boltzmann algorithm is advanced 500 time steps and the macroscopic properties are averaged over the 200 last time

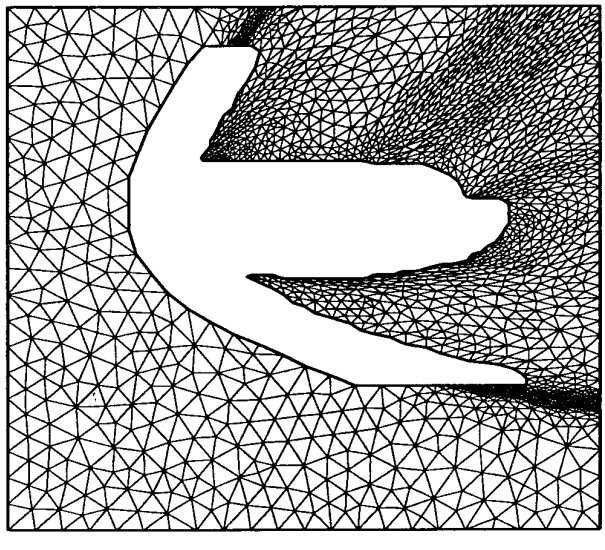

FIG. 12. The Navier–Stokes mesh used for computing the coupled solution.

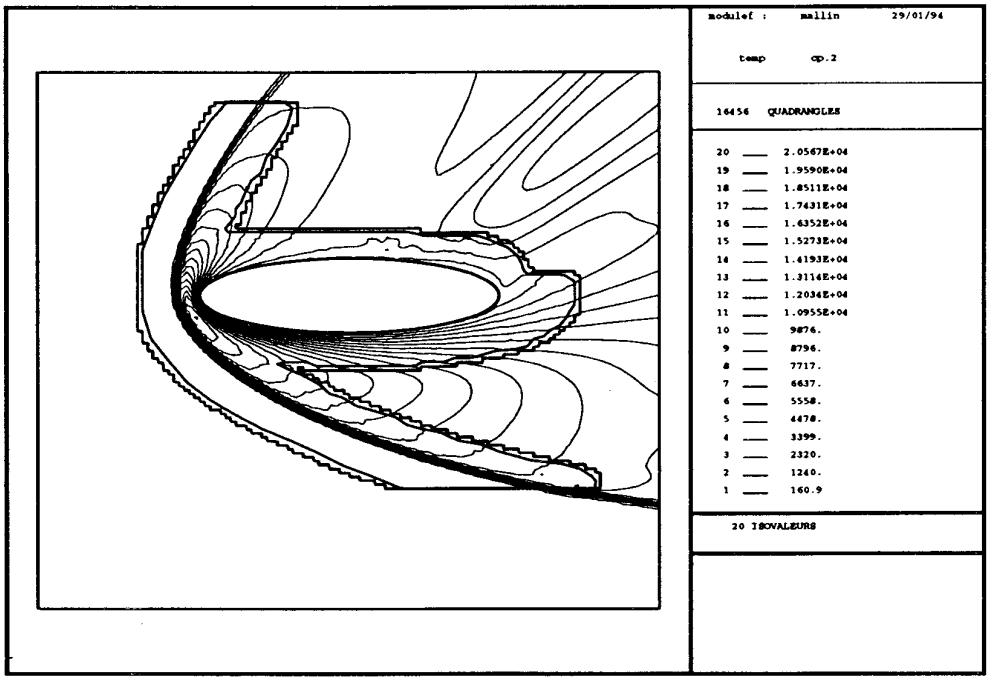

FIG. 13. Isolines of the temperature for the coupled solution. The Boltzmann domain is around the body. The smooth interface represents the internal boundary of the Navier–Stokes region.

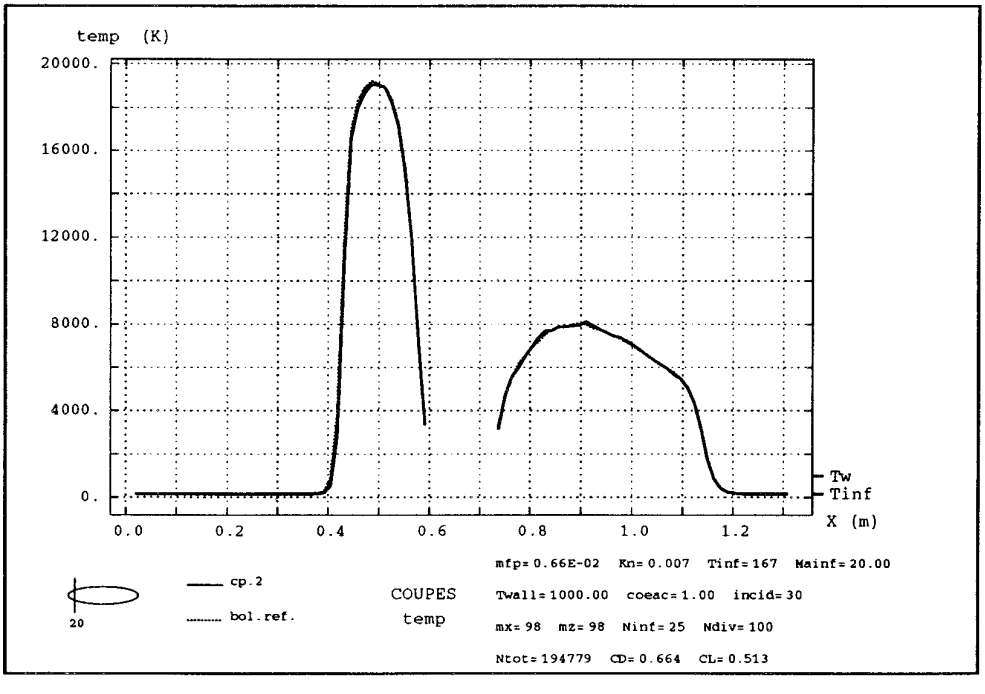

FIG. 14. Temperature cross sections of the coupled solution (continuous line) and of the Boltzmann reference solution (dotted line). The section is shown at the left bottom of the figure.

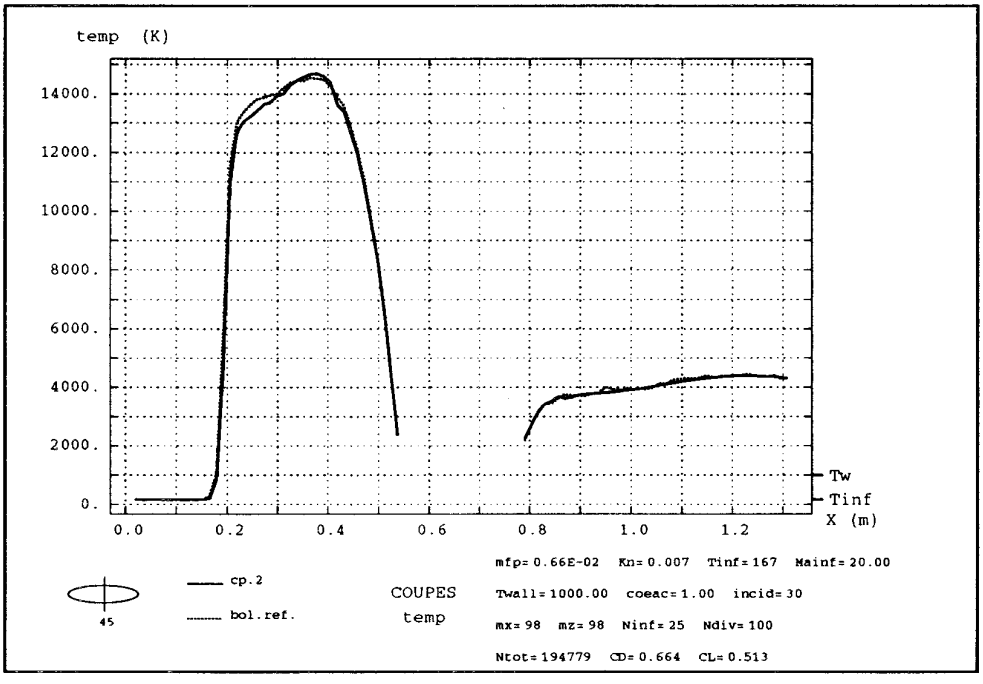

FIG. 15. Temperature cross sections.

steps. Concerning the computational time, on a typical workstation, a gobal coupled iteration needs 1 *h* corresponding to 30 *mn* for each solver. The global residual, computed according to formula (21), is stable after three global iterations. Figure 13 represents the temperature isolines. The continuity at the interface is very good. We want to recall here that we do not impose variable continuity at the interface but only half fluxes. This property is still observed on the other isolines (mach number, density, ...). Figures 14 and 15 represent two cross sections of the temperature, superimposed with a Boltzmann reference solution. We can remark that the superposition is very good. Moreover, the coupled solution recovers the right temperature jump at the body. Finally, Figs. 16 and 17 show respectively the heat flux coefficient C_h and the skin friction coefficient *Cf*. The above coefficients are given by the formulas

$$C_f = \frac{(\sigma \cdot n) \cdot \tau}{0.5\, \rho_\infty u_\infty^2},$$

$$C_h = \frac{(q \cdot n)}{0.5\, \rho_\infty u_\infty^3}.$$

For these last results the superposition of a coupled Boltzmann solution and the coupled solution is very good except for the heat flux coefficient in a region under the body. This small error is certainly due to the bad position of the corresponding interface on which we impose our incoming Maxwellian distribution for the Boltzmann problem.

7.2. *Flow around a Plate*

In this section we show that the coupling algorithm leads to a gain of CPU time, compared to a standard Boltzmann algorithm used in the whole space domain, if the gas is ''sufficiently dense.'' The different solutions are computed on a HP735 station.

The first test case computes an external flow around a plate of length 0.1 m, without an angle of attack. The parameters of the flow are

$$\begin{aligned} M_\infty &= 18.33, & T_W &= 290\ \text{K}, \\ T_\infty &= 13.6\ \text{K}, & \gamma &= 5/3, \\ u_\infty &= 1503.5\ \text{m/s}, & \text{Pr} &= 2/3, \\ \rho_\infty &= 1, & \text{Re}_{/\text{m}} &= 30211. \end{aligned}$$

We have computed three global coupled iterations. The Navier–Stokes mesh is shown on Fig. 18. The computational time for one global Boltzmann iteration is 10 mn for 500 time steps. For one global Navier–Stokes iteration the time is 8 mn for 700 explicit time steps. Thus the total time of computation is 54 mn for the coupled solution. The Boltzmann reference solution is obtained after 1500

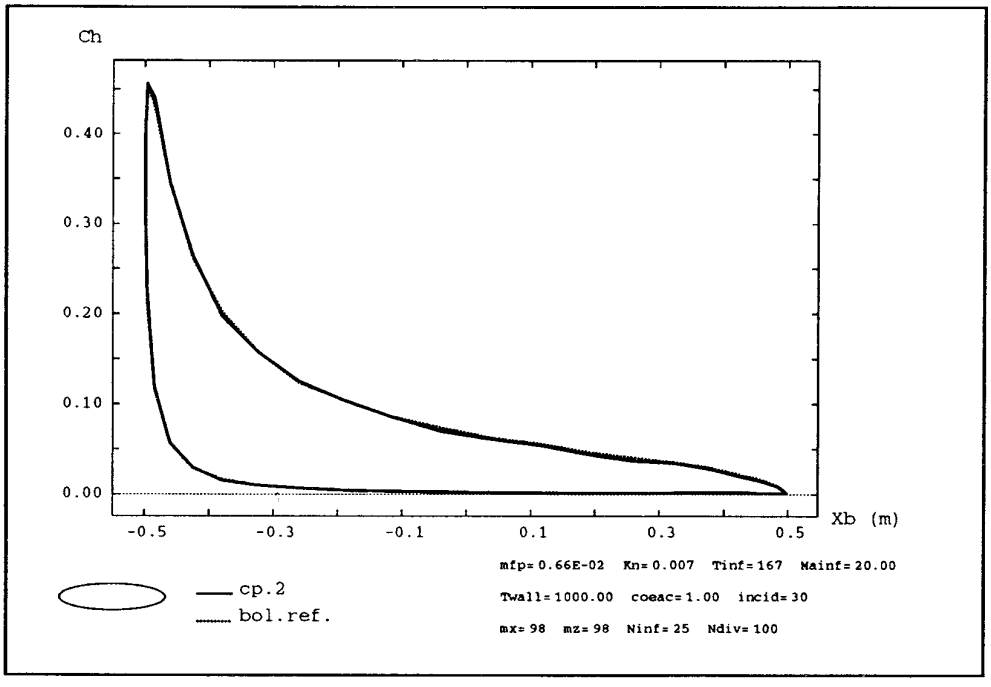

FIG. 16. Heat flux coefficient C_h of the coupled solution (continuous line) and of the Boltzmann reference solution (dotted line).

time steps. The corresponding time of computation is 1 h 04 mn. Thus, for this test, both computation times are comparable. It seems that the coupling algorithm has no advantage for this case.

Before going to another test case it may be interesting to analyse some results. Figure 19 shows the isolines of the density of the coupled solution. The continuity is good. Figures 20 and 21 are cross sections of the density and the

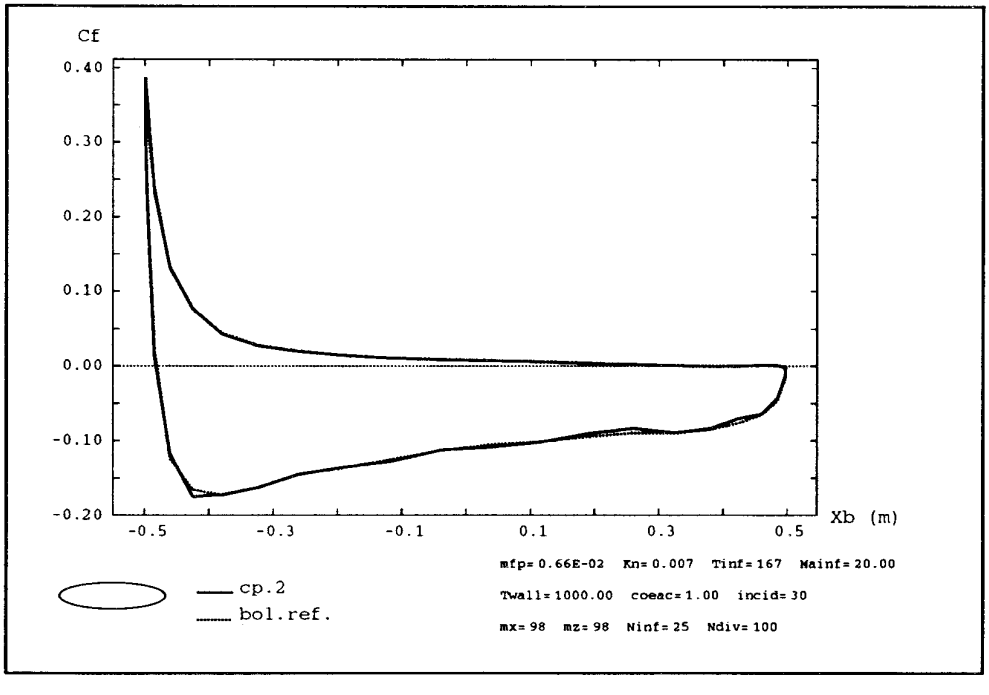

FIG. 17. Skin friction coefficient *Cf* of the coupled solution (continuous line) and of the Boltzmann reference solution (dotted line).

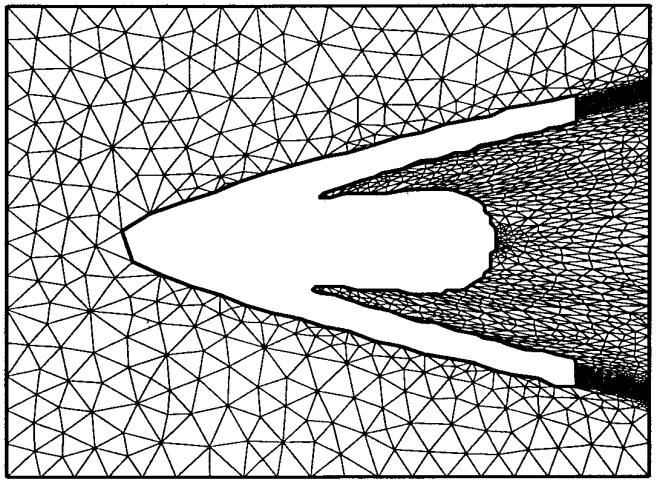

FIG. 18. Navier–Stokes mesh to compute a coupled solution around a plate.

temperature. The direction of the cross section is perpendicular to the direction of the plate. We have superimposed three different solutions; the coupled solution (dotted line), the Boltzmann reference solution (thin continuous line), and a Navier–Stokes solution computed in the whole domain with no slip condition and imposed temperature on the plate. For both the temperature and the density the superposition of the Boltzmann reference solution and the coupled solution is very good. On the other hand, the Navier–Stokes solution is very bad; the shock is displaced and we observe a jump of temperature at the plate. Similarly, we observe a jump of the density at the plate. We see on this example that the Navier–Stokes model with no slip and imposed temperature on the body is a poor alternative to compute such flows.

The last test case we have performed is similar to the previous one except that the Reynolds number per meter is now equal to 60421. The Boltzmann reference solution is obtained after 2000 time steps corresponding to 5 h 30 mn of computational time. For the coupled solution we have used five global iterations. One global Boltzmann iteration is obtained computing 400 time steps, after 18 mn and the global Navier–Stokes iteration is obtained computing 700 explicit time steps, after 12 mn. Thus the global time of computation for the coupled solution is 2 h. In this case the coupling algorithm leads to a smaller computational time.

8. CONCLUSION

We have proposed in this paper a numerical adaptative coupling strategy to solve hypersonic flows, at high speed, around a vehicle. Our strategy includes an automatic definition of the computational Navier–Stokes and Boltzmann domains. To this end we have introduced the Grad criterion which measures the distance between the Navier–Stokes and the Grad thirteen moments solutions. The coupling is achieved by a natural matching of half fluxes at

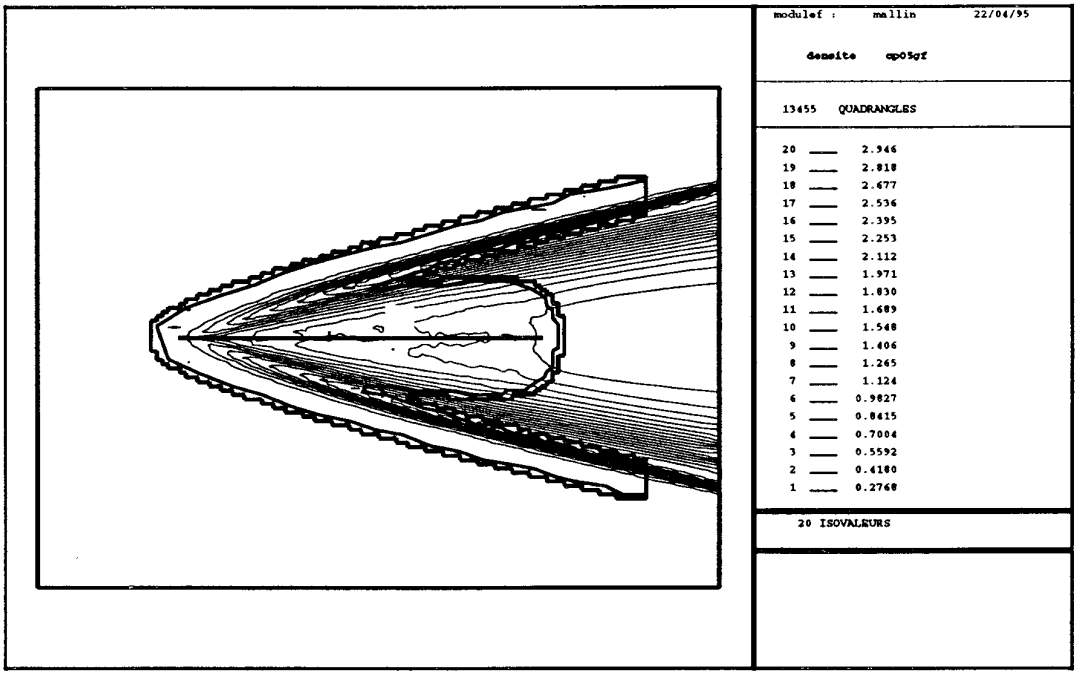

FIG. 19. Isolines of the density.

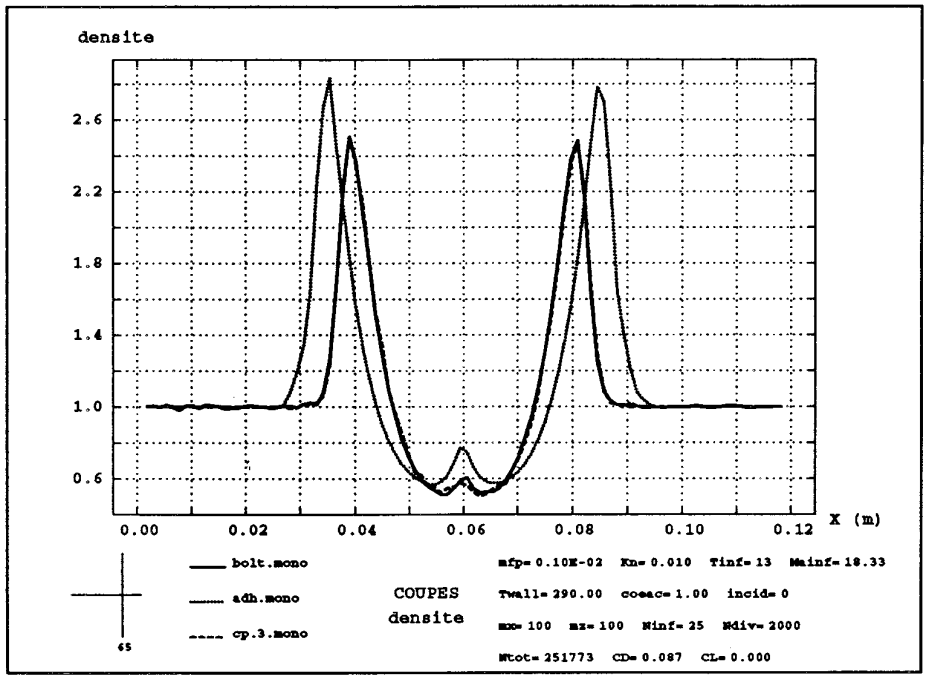

FIG. 20. Cross sections of the density (Navier–Stokes, Boltzmann, and coupled).

the interface of the domains. The Boltzmann and the Navier–Stokes solver are coupled by a time marching algorithm. The resulting strategy is very flexible; each step is solved by its own code.

However, our strategy has two weaknesses. First, there is no systematic strategy to determine the threshold criterion value in the domain construction. Moreover, we cannot estimate a priori, from a theoretical point of view, the

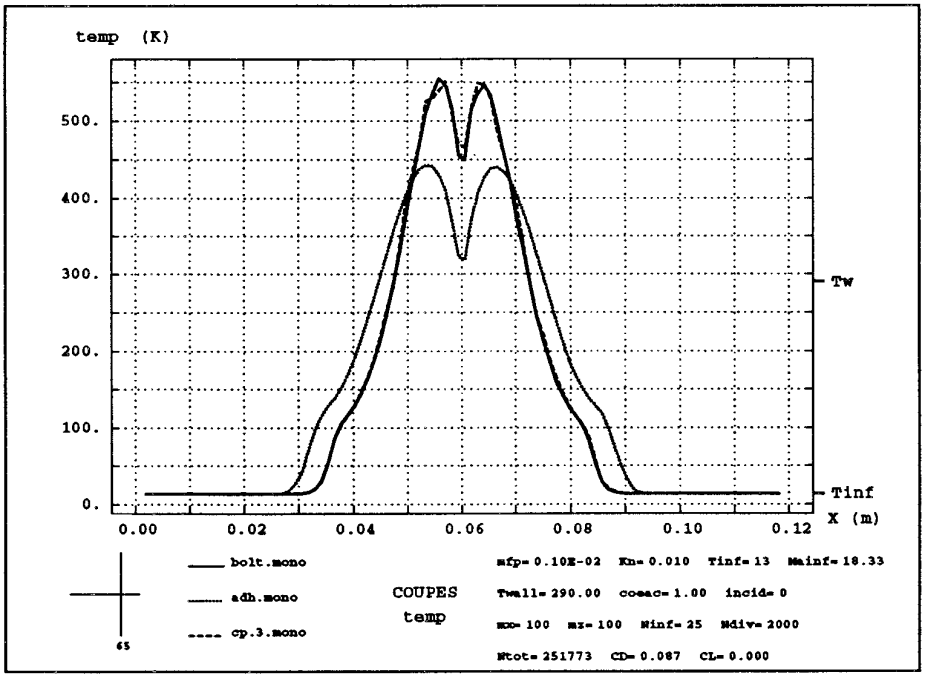

FIG. 21. Cross sections of the temperature (Navier–Stokes, Boltzmann, and coupled).

number of time steps for each global Boltzmann and Navier–Stokes coupling iteration. All these values are determined in an empirical way.

Nevertheless, our numerical results are very satisfactory, compared with Boltzmann reference solutions. The isoline continuity is preserved at the interface. Moreover, thanks to the criterion, we can optimize the Boltzmann computational domain. The global strategy leads to a good gain of time. In addition, our method may be extended to 3D calculations and to more complex gases, involving multispecies, rotational temperature [20], and possibly chemistry and vibrational temperature. The last case requires us to study the transition from microscopic to macroscopic models in the presence of strong disequilibrium in molecular internal vibrational energy.

REFERENCES

1. H. Babovsky, On a simulation scheme for the Boltzmann equation, *Math. Methods Appl. Sci.* **8,** 223 (1986).
2. H. Babovsky and R. Illner, A convergence proof for Naubu's simulation method for the full Boltzmann equation, *SIAM J. Numer. Anal.* **26** (1), 45 (1989).
3. G. A. Bird, *Molecular Gas Dynamics and the Direct Simulations of Gas Flows,* Clarendon Press, Oxford, 1994.
4. J.-F. Bourgat, P. Le Tallec, and M. D. Tidriri, Coupling Boltzmann and Navier–Stokes by Friction, *J. Comput. Phys.,* **127,** 227 (1996).
5. J. F. Bourgat, P. Le Tallec, F. Mallinger, Y. Qiu, and M. Tidriri, "Numerical coupling of Boltzmann and Navier-Stokes," in *Proceedings of the IUTAM Conference on Rarefied Flows for Reentry Problems, Marseille France, Septembre 1992.*
6. R. Brun, *Transport et relaxation dans les écoulements gazeux* (Masson, Paris, 1986).
7. C. Cercignani, *The Boltzmann Equation and Its Application* (Springer-Verlag, New York/Berlin, 1988).
8. T. Chan, R. Glowinski, J. Periaux, and O. Widlund (Eds.), *Proc. Second Int. Symp. on Domain Decomposition Methods for Partial Differential Equations, Los Angeles, CA, January 1988* (SIAM, Philadelphia, 1988).
9. S. Chapman and T. G. Cowling, *The Mathematical Theory of Nonuniform Gases* (Cambridge Univ. Press, Cambridge, 1990).
10. L. Desvillettes, P. Herrera, and E. Raymundo, A vectorizable simulation method for the Boltzmann equation, *Meth. Math. Num. Anal.* **28,** 745 (1994).
11. F. Gastaldi and L. Gastaldi, On a domain decomposition approach for the transport equation: theory and finite element approximations, *IMA J. Numer. Anal.* **14** (1993).
12. F. Gastaldi, A. Quarteroni, and G. Sacchi Landriani, On the coupling of two-dimensional hyperbolic and elliptic equations: Analytical and numerical approach, *in* [8].
13. H. Grad, On the kinetic theory of rarefied gases, *Comm. Pure Appl. Math.* **2** (1949).
14. R. Gupta, C. Scott, and J. Moss, "Slip-Boundary Equations for Multicomponent Nonequilibrium Airflow," *NASA Technical Paper* 2452, November 1985.
15. R. Illner and H. Neunzert, On simulation methods for the Boltzmann equation, *Transp. Theory Stat. Phys.* **16,** 2/3, 141 (1987).
16. P. Le Tallec, "Domain decomposition methods in computational mechanics," in *Computational Mechanics Advances, Vol. 1, No. 2,* February 1994.
17. D. Levermore, "Moment Closure Hierarchies for Kinetic Theories," Draft 29, 1993.
18. A. Lukshin, H. Neunzert, and J. Struckmeier, "Coupling of Navier–Stokes and Boltzmann Regions," *Interim Report for the Hermes Project DPH 6174/91,* 1992.
19. R. Illner and J. Struckmeier, Boundary value problems for the steady Boltzmann equation, *J. Statist. Phys.* **85,** 427 (1996).
20. F. Mallinger, "Couplage adaptatif des équations de Boltzmann et de Navier-Stokes," *Thèse de l'Université de Paris IX Dauphine,* September 1996.
21. M. Mallet, "A Finite Element Method for Computational Fluid Dynamics," *Ph.D. thesis,* Stanford University, 1985.
22. K. Nanbu, Direct simulation scheme derived from the Boltzmann equation. I. Monocomponent gases, *J. Phys. Soc. Japan* **49,** 2042 (1980).
23. H. Neunzert, F. Gropengiesser, and J. Struckmeier, Computational methods for the Boltzmann equation, in *Applied and Industrial Mathematics,* edited by R. Spigler (Kluwer Academic, Dordrecht, 1991), p. 111.
24. B. Perthame, Introduction to the theory of random particle methods for the Boltzmann equation, in *Advances in Kinetic Theory and Computing: Selected Papers, 1994.*
25. F. Shakib, *Finite Element Analysis of the Compressible Euler and Navier–Stokes Equations, Ph.D. thesis,* Stanford University, 1988.
26. F. Shakib, T. J. R. Hughes, and Z. Johan, A multielement group preconditioned GMRES algorithm for nonsymmetric systems arising in finite element analysis, *Comput. Methods Appl. Mech. Engrg.* **75** (1989).
27. J. Struckmeier and K. Steiner, A comparison of simulation methods for rarefied gas flows, Preprint 91, Arbeitsgruppe technomathematik, Univ. Kaiserslautern, 1993.
28. G. V. Walter Vicenti and C. H. Kruger, *Introduction to Physical Gas Dynamics* (Krieger, Melbourne, FL, 1986).
29. X. Zhong, R. W. MacCormack, and D. R. Chapman, Stabilization of the Burnett equations and application to hypersonic flows, *AIAA J.* **31,** 6 (1993).